

FENG, J., PAN, Y., YANG, M., FERNANDEZ, C., CHEN, X. and PENG, Q. [2021]. A lactoglobulin-composite self-healing coating for Mg alloys. *ACS applied bio materials* [online], Articles ASAP. Available from:
<https://doi.org/10.1021/acsabm.1c00560>

A lactoglobulin-composite self-healing coating for Mg alloys.

FENG, J., PAN, Y., YANG, M., FERNANDEZ, C., CHEN, X. and PENG, Q.

2021

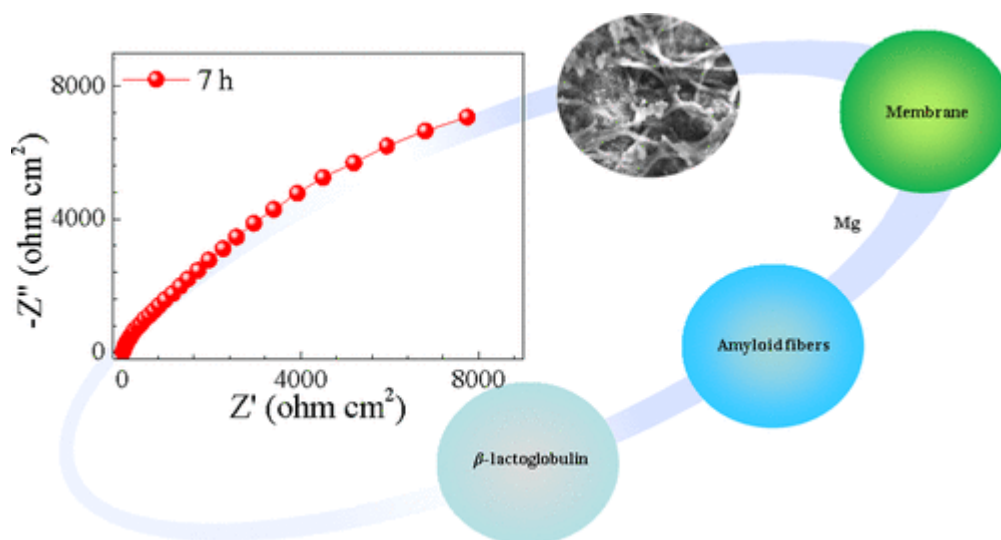
This document is the Accepted Manuscript version of a Published Work that appeared in final form in ACS Applied Bio Materials, copyright © American Chemical Society after peer review and technical editing by the publisher. To access the final edited and published work see
<https://pubs.acs.org/doi/10.1021/acsabm.1c00560>.

A Lactoglobulin-Composite Self-Healing Coating for Mg Alloys

Jiawen Feng, Yukun Pan, Meng Yang, Carlos Fernandez, Xiaobo Chen, and Qiuming Peng*

ABSTRACT: Corrosion issue is one of the most crucial bottlenecks for extensive employment of Mg alloys, in particular under harsh engineering conditions. Differing from traditional approaches, a self-healing protective coating composed of lactoglobulin is proposed herein to offer sustainable protection to the underlying Mg parts. Corrosion resistance, evaluated by electrochemical measurements and hydrogen evolution tests, indicates that the lactoglobulin composite film exhibits nobler corrosion potential ($-1.28 V_{SCE}$), smaller corrosion current density ($8.4 \times 10^{-6} A/cm^2$), and lower average corrosion rate ($\sim 0.03 mm/y$) than those of its bare counterparts. Moreover, the pre-made cracks in the film were evidently self-healed within 24 h of exposure to corrosive media. The proposed self-healing lactoglobulin composite film provides opportunities to tackle the corrosion challenges of Mg alloys.

KEYWORDS: magnesium alloy, β -lactoglobulin, coating, corrosion properties, self-healing



INTRODUCTION

Magnesium (Mg) alloys have widespread application prospects in aerospace, electronics, automotive, and medical industries owing to their low density, high specific strength, and promising biocompatibility.¹⁻³ However, as an active element, Mg alloys are prone to corrosion and oxidation, which severely limits their widespread applications.^{4,5} As such, proper surface treatment is essential to tackle the corrosion challenge. Currently, the prevalent surface treatment methods include chemical conversion,^{6,7} anodization,^{8,9} acid treatment,¹⁰ micro-arc oxidation,¹¹⁻¹³ metal plating,¹⁴ and polymer coating.¹⁵ Through proper surface treatment techniques, a protective film can be formed on the surface as a physical barrier to effectively isolate the underlying Mg alloys from corrosive attack, and thus corrosion resistance is improved. However, once the physical integrity of the barrier coatings fades, the underlying Mg parts will be exposed to corrosive media and form galvanic couples with surrounding intact sites, which will accelerate corrosion.¹⁶ In this regard, coatings with self-healing functions on demand are highly desirable to provide sustainable protection to Mg alloys.

Inspired by the spirit of skin regeneration, a variety of self-healing coating strategies have been attempted. Cheng's¹⁷ research group prepared a self-healing coating on the surface of the Mg-1Ca alloy by synthesizing fibroin, using K_3PO_4 as a corrosion inhibitor and adjusting the secondary structure of fibroin, which was conducive to osteogenesis and achieved wonderful self-healing. Zhou et al.¹⁸

reported improved corrosion resistance of Mg alloys through a multifunctional self-healing coating consisting of carboxylic acid and fluoropolymer nano-containers, which can control the corrosion inhibitors to heal the scratched area. Zhu et al.¹⁹ studied a chitosan/hyaluronic acid polyelectrolyte coating whose service life is extended through an evident self-healing function. Unfortunately, the self-healing ability is at the expense of interfacial adhesion between the coating and substrate.¹⁷ Moreover, the responsive kinetics is too slow to provide prompt and continuous restoration of defects in the coating, which is ascribed to the weak reaction between the film and matrix.¹⁷

Protein is a biological macromolecule with a large number of oxygen-containing functional groups, which adsorbs some isolated metallic ions or alloys,²⁰ and under the conditions of destroyed adsorption interface, it is able to form a fresh adsorption layer, i.e., self-healing ability.²¹ Furthermore, the structure of a protein contains N atoms, which can provide lone pairs of electrons and have a certain corrosion inhibitory effect on metals.²² The nitrogen could coordinate with metal ions using its lone electron pair to form chelates, which inhibits the corrosion of metals. The metal cation can complex carboxyl groups in proteins to form insoluble salts. At this time, the hydrophilic groups in each protein monomer are located inside the protein molecule, while the major hydrophobic residues are exposed on the surface of the molecule.²³ Therefore, a hydrophobic film can be formed on the metal surface. In addition, the secondary bond is destroyed, and the protein molecule changes from the original ordered curly structure to the disordered stretched structure, forming nanofibers with certain mechanical properties.²⁴ In summary, using a protein to improve the corrosion resistance of the metal, not only simplifies the experimental procedure but also increases the adhesion force between the metal and the protein.

Herein, taking pure Mg as a material model, we prepared a β -lactoglobulin protein composite film, which shows a high anticorrosion ability in combination with a unique self-healing function. β -Lactoglobulin, as an edible protein, is the main component of whey protein. Its molecular weight is about 18.3 kDa and the isoelectric point is in the range of 5.1–5.3. Its monomer consists of 162 amino acids with a large number of oxygen-containing functional groups.²⁵ Compared to other proteins, β -lactoglobulin is more readily converted into amyloid fibrils.²⁶ When the metal is immersed in the β -lactoglobulin solution, the metal ions can break the strong hydrogen bonds between β -lactoglobulin molecules and induce the polymerization of β -lactoglobulin into fibrous aggregates. After the metal surface film is destroyed, the free metal ions can reattach the fibrous aggregates to the metal surface, which makes the protein have a self-healing function.

EXPERIMENTAL PROCEDURES

Sample Preparation. Pure Mg was used to explore the anticorrosive properties of the proposed composite film. Cylindrical samples with a diameter of 8 mm and a height of 3 mm were cut as the substrate and then mechanically polished. The samples were cleaned with deionized water and ethanol and then dried at room temperature (RT). As shown in [Scheme 1](#), Mg specimens were first immersed in 0.1% hydrochloric acid solution for 5 min, rinsed with deionized water, and dried at RT. Subsequently, the specimens were immersed in a prepared aqueous solution containing β -lactoglobulin (0.25 wt %) for 2 h, then taken out, washed with deionized water, and dried at RT for 2 h. The alloy which was treated with hydrochloric acid together with protein was denoted as H-P-Mg. For comparison, two references which were treated under the same experimental conditions were involved: (i) Mg was only mechanically polished, without surface treatment (denoted as Mg) and (ii) the polished Mg was directly immersed in 0.25 wt % β -lactoglobulin solution for 2 h (denoted as P-Mg). In addition, β -lactoglobulin was extracted directly from cow milk. First, 10 g of cow milk powder was taken and dissolved in 90 g of ultrapure water by magnetic stirring. Then, the pH was adjusted to 4 using concentrated hydrochloric acid, followed by heating in a water bath at 40 °C for 8 h. In the last step, it was centrifuged to recover the supernatant and β -lactoglobulin powder was finally obtained after freeze-drying. When preparing protein solution, β -lactoglobulin powder was dissolved in ultrapure water, and the pH was tuned to 2.

Surface Analysis. Phase compositions have been identified by X-ray diffraction (XRD), in which the tests were carried out over a range from 5 to 60° at a speed of 4 °/min. Surface morphologies and elemental compositions were investigated using a field emission scanning electron microscope (FESEM) equipped with an energy dispersive spectrometer (EDS). An accelerated voltage of 20 kV was used. In addition, X-ray photoelectron spectroscopy (XPS) was conducted on a Thermo Fisher X-ray photoelectron spectrometer with Al K α (1486.6 eV). The binding energies obtained in XPS analysis were calibrated by referring to the C 1s peak position (284.5 eV) and the F 1s peak position (685.7 eV).

Electrochemical Tests. The electrochemical tests were reported in our previous work.²⁷ Corrosion behavior was characterized by immersion tests of plug-in specimens in 0.9 wt % NaCl aqueous solution using open circuit potential (OCP), polarization curves, electrochemical impedance spectroscopy (EIS), and hydrogen evolution. The 0.9 wt % NaCl solution was used as the electrolyte solution to simulate the body fluid. The OCP measurement was performed immediately after immersing the specimens in NaCl solution, and this was continued for 3 h. The polarization curves were recorded from -2.0 to -0.5 V (vs saturated calomel electrode (SCE)) after immersing the samples for 3 h. The polarization curves were continuously scanned three times to observe average corrosion resistance and the recovery ability of the composite film when it was destroyed. In addition, EIS spectroscopy corresponding to samples immersed in the NaCl solution for 3, 5, and 7 h, respectively, was performed. Each group of samples was tested three times in parallel. All electrochemical tests were recorded using a potentiostat/frequency response analysis system (Bio-logic, VSP), and fitted using EC-Lab software.

Hydrogen Evaluation Tests. Hydrogen evaluation was recorded by immersing in the 0.9 wt % NaCl solution at RT for a recording period of 120 h. Each condition was tested in triplicate to reduce experimental error. The corrosion properties were evaluated by an instantaneous corrosion rate (Pi), hydrogen evolution rate (PH) during corrosion, and weight loss corrosion rate (Pw).⁴ Moreover, the corrosion products were removed with chromic acid (20 g of chromium trioxide, 2 g of barium nitrate, and 1 g of silver nitrate dissolved in 100 mL of deionized water).

Self-Healing Capability Evaluation. The self-healing role of the lactoglobulin composite film was examined by a scratch test using the Revetest Scratch Tester (CSM RST). The scratch test method used a diamond indenter to slide on the surface of the alloy. During this process, an automatic loading mechanism was used to continuously apply a vertical load. A needle tip with a diameter of 10 μm and a force of 100 N has been used to draw a cruciform scratch on the surface of the alloy. The width of the scratch was measured to be ~ 150 μm . SEM observations were used to perceive the morphology variation of scratches. The self-healing test has been performed in 0.9 wt % NaCl solution for up to 96 h.

RESULTS AND DISCUSSION

Film Characteristics. The surface of pure Mg is smooth at a resolution of 50 μm (Figure 1a), whereas a high resolution (1 μm) reveals a loose morphology (Figure 1b). In the case of PMg, several nano-sized fibers and a large number of nano-sized pores scatter over the surface (Figure 1c,d). Comparatively, a uniform network structure is witnessed on the surface of H-PMg, wherein a large number of nano-sized amyloid fibers are observed (Figure 1e,f). In addition, the thickness of the lactoglobulin film is 2.69 ± 0.02 μm for P-Mg, while it is thickened up to 2.74 ± 0.02 μm for the H-P-Mg sample (Figure 1g,h), indicating that a rough metal surface can bind more lactoglobulin. As seen in Figure 1i, the peaks of Mg exit in all samples, yet the amorphous diffraction peak at $10\text{--}12^\circ$ in both P-Mg and H-P Mg is broad, which can be related to the formation of the lactoglobulin composite film.²⁸ Since N is one of the main elements of lactoglobulin, the amount of β -lactoglobulin can be correlated to the content of N linearly. As summarized in Figure 1j, the lactoglobulin content is in the order of H-P-Mg > P-Mg > Mg. Specifically, hydrochloric acid treatment improves the roughness of the alloy surface and increases the adsorption capacity of lactoglobulin.

Electrochemical Measurements. OCP was monitored and plotted as a function of voltage and immersion time (Figure 2a). For pure Mg, the OCP value is continuously increased with immersion time and the potential decreases sharply at 1.7 h. The origin can be ascribed to the fact that as the immersion time increases, a loose magnesium hydroxide film is formed on the surface of the alloy, which slightly prevents the corrosion from Cl^- . When magnesium hydroxide falls off, new metal magnesium is exposed, causing fluctuations of the potential. On the contrary, the OCP value of P-Mg is also increased with time, accompanied by severe fluctuations. It takes ~ 2.2 h to reach the equilibrium potential. Attractively, H-P-Mg takes less than 5 min to reach the equilibrium potential of -1.563 V_{SCE} . This underlines that the adsorption amount of Cl^- on the interface of the lactoglobulin coating is lower than that of the bare substrate, indicating that H-P-Mg further reduces the adsorption of Cl^- .

Figure 2b–d shows the potentiodynamic polarization curves of different samples. Corresponding parameters depending on the Tafel slope fitting are listed in Table 1. Membrane breakdown potential platforms in the initial anode branch are observed in Mg and P-Mg samples, which indicate that the

surface oxidation film was not intense and the penetration of corrosive media cannot be effectively prevented (Figure 2b,c). As far as H-P-Mg is concerned, similar vertical anode branches are detected and the current density increases in a small range with increasing electrode potential (Figure 2d). This implies that the formed lactoglobulin composite film is compact, and the lactoglobulin composite film could be rapidly regenerated after being destroyed by a large polarization current during the polarization cycle tests, a prerequisite to achieving the self-healing function.

To probe the corrosion process, the Nyquist curves and Bode diagrams were recorded. Both Mg and P-Mg samples (Figure 3a,b) exhibit a high-frequency capacitive loop, as well as a distorted inductive loop in the low frequency. The corresponding Bode diagrams show that there appear to be two time constants in H-P-Mg and the other samples have only one time constant. As the frequency increases, the impedance value of Mg first increases and then decreases, mainly due to the dissolution of the alloy surface and the corrosion products formed on the surface which play an obstructive role and promote more oxide film rupture (Figure 3d). For P-Mg, the resistance value decreases with the increase of the test time, which is mainly because the noncompact composite coating promotes the corrosion of Cl⁻ and accelerates the corrosion rate (Figure 3e). In turn, there was only a capacitive semi-circle observed for H-PMg, indicating that the lactoglobulin composite film is strongly compact to prohibit the penetration of the solution (Figure 3c). H-P-Mg shows the largest phase angle at lower frequencies, which elucidates the capacitance performance with good dielectric properties (Figure 3f).

The equivalent circuit is obtained by fitting the Nyquist diagram (Figure 3g,h), where R_s represents the solution resistance, R_{c1} is the coating resistance of the natural oxide film (Mg) and the whole film (P-Mg), R_{c2} is the coating resistance of H-P-Mg, and R_{ct} and R_L represent the charge transfer resistance and the inductance resistance, respectively. The CPE_1 and CPE_{dl} describe constant phase elements, characterizing the nonideal resistive and capacitive behavior of specimens. The mathematical model of CPE is expressed as follows

$$Z_{CPE} = \frac{1}{Y(j\omega)^n} \quad (1)$$

where Y is admittance; j is the imaginary unit; ω is the angular frequency; and n is designated as the dispersion coefficient of CPE. When the value of n is 1, CPE can be regarded as a capacitor; when the value of n is zero, CPE can act as a resistor. Table 2 shows the results of EIS fitting. To some extent, the impedance value at low frequencies (particularly 0.01 Hz) corresponds to the impedance of the sample, which reflects the degree of corrosion. Generally, a higher R_{ct} value represents a lower dissolution rate and higher corrosion resistance ability. The polarization resistance of the H-P-Mg gradually increases with the extension of the immersion time, indicating that the corrosion rate of the alloy gradually decreases with the extension of time. In addition, H-P-Mg has the largest fitting charge transfer resistance (R_{ct}), and the R_{ct} value reaches $\sim 1.6 \times 10^4$ ohm cm^2 even after soaking for 7 h. The higher R_{ct} value of H-PMg reflects that the coating greatly improves the corrosion resistance of Mg.

Corrosion Behavior. The corrosion potential (E_{corr}) and the average corrosion rate (P_i) of the samples have been calculated based on the Tafel polarization curves (Table 1). In general, the higher corrosion potential and lower corrosion current density indicate better corrosion protection. Compared with the other two samples, the E_{corr} of the H-P-Mg is the most positive ($-1.28 V_{SCE}$). The instantaneous corrosion rate is ~ 0.03 mm/y, much lower than those of super-high purity Mg of ~ 0.25 mm/y⁴ and high purity Mg of ~ 0.38 mm/y,²⁹ which is only $\sim 6\%$ of that for pure Mg. The weight loss and hydrogen evolution are further determined to evaluate the corrosion degree. All samples were immersed in static 0.9 wt % NaCl solution for 6 days. As shown in Figure 4a, in the beginning, the lactoglobulin composite film of the H-P-Mg is relatively stable without any bubbles on the surface. Hydrogen has not been collected either. The rate of hydrogen evolution is gradually increased after 5 h, and it reaches its maximum at about 72 h and then drops slowly (Figure 4b). The process is totally different from the other two samples, wherein the hydrogen evolution rate increased rapidly in the initial stage and then remains stable. The weight-loss corrosion rate (P_w) of the H-P-Mg is ~ 0.75 mm/y, which is about one-fifth that for Mg (Figure 4c). As shown, the corrosion resistance ability is in the order of P-Mg < Mg < H-P-Mg. To elucidate the mechanism of the lactoglobulin film in the corrosion process, ex situ SEM observation was performed after immersing it for different time intervals. Figure 5a–c reveals that pitting pits

appeared on the surface of the bare Mg sample after immersing for 5 min. With increasing immersion time, a large number of cracks occur on the surface, and the corrosion products become loose and porous. Comparatively, finite cracks are also observed on the surface of the lactoglobulin composite film (Figure 5d–f). However, as the immersing test proceeds, the cracks are gradually filled with the corrosion products. More importantly, the width of the slits is slowly eliminated and the film becomes more compact.

The surface morphologies of the alloys after removing the corrosion products are shown in Figure 6. The surface of bare Mg (Figure 6a–b) has a large number of holes and the diameter of pores is $\sim 0.6 \pm 0.1 \mu\text{m}$. Conversely, the H-P-Mg (Figure 6d–e) shows a relatively flat substrate, in which a few small holes are mainly related to hydrochloric acid corrosion. The cross-section observations (Figures 6c,f) reveal that the depth of the pitting position for bare Mg is $\sim 78 \mu\text{m}$, but it is $\sim 32 \mu\text{m}$ for the H-PMg. The results show that the complexation of lactoglobulin and metal ions successfully forms an excellent physical barrier, effectively improving the corrosion resistance of Mg.

Self-healing Behavior. A scratch immersion test has been performed to probe the self-healing process. Figure 7 shows the morphology variation of the oxidation film in NaCl solution. For bare Mg (Figure 7a), after 24 h of soaking, a large amount of $\text{Mg}(\text{OH})_2$ accumulates on the surface of Mg and obvious scratches can be observed. In conjunction with Figure 6b, during immersion corrosion, pores are generated on the Mg matrix, resulting in loose and porous accumulation of corrosion products. After 96 h of immersion, the scratches are still visible. In contrast, the scratches on the H-P-Mg surface become very shallow after 24 h of immersion, and the corrosion products are uniformly spread on the surface of H-P-Mg (Figure 7b). After 96 h of immersion, the scratches are almost gone, however, corrosion products still exist which become more dense. Apparently, the lactoglobulin composite film bestows self-healing ability.

XPS measurement has been conducted to study the chemical composition variation of the film (Figure 8a). It is seen that almost no Mg matrix is observed for the Mg sample treated in lactoglobulin solution, demonstrating that a compact lactoglobulin composite film is formed on the surface. Differing from the pure Mg (Figure 8b), some new peaks, such as those of the C=O group ($\sim 287.8 \text{ eV}$, Figure 8c), N–H group ($\sim 399.9 \text{ eV}$), and N–O group (403.0 eV) (Figure 8d), are detected in H-P-Mg. Figure 9 shows the high magnification images of C 1s, O 1s, and Mg 1s. Compared with Mg, two different characteristics have been confirmed. One is that new valences of O and C, such as O^{2-} and COO^- , have been found (Figure 9a,b). The other is the weak Mg^{2+} peak (Figure 9c). Overall, lactoglobulin contains a large number of oxygen-containing functional groups, which can interact with Mg^{2+} to establish cross-linking and also have a certain coagulation effect on lactoglobulin, forming a dense coating. Since protein is an amphoteric polymer, after the hydrophilic group captures the divalent magnesium ions for complexation, the hydrophobic groups of the protein are rotated and exposed on the metal surface, thereby making the coating hydrophobic. As shown in Figure 10, H-P-Mg has a larger water contact angle (108.24°) than Mg (49.72°) and P-Mg (67.68°), proving that it has a strong hydrophobic effect. So the improved anticorrosion property is closely related to the chelation between lactoglobulin and Mg. Figure 11 shows a schematic diagram of the anticorrosion and self-healing mechanisms of the protein-containing composite film. Specifically, a large amount of Mg^{2+} and some Cl^- are present on the surface of the alloy after rinsing with hydrochloric acid (Figure 11a). Subsequently, the sample is immersed in the lactoglobulin solution (Figure 11b) and the lactoglobulin adsorbs Mg^{2+} to form a fiber-like film and is uniformly attached to the surface of the substrate. In the following corrosion testing, as soon as the cracks appear on the surface (Figure 11c), the fresh matrix is exposed to the solution. Thus, some new Mg^{2+} ions could be exposed. Owing to the presence of carboxyl groups or amino groups in lactoglobulin, the isolated Mg^{2+} ions would be chelated to form a new lactoglobulin composite coating covering the original coating surface (Figure 11d,e). This makes the Mg not only have good corrosion resistance but also good self-healing properties.

CONCLUSIONS

Based on the unique reaction characteristics between protein and metal ions, a network structure lactoglobulin composite film method. The lactoglobulin composite film demonstrates outstanding anticorrosion properties and a promising self-healing behavior. The formation and self-healing mechanisms of the lactoglobulin composite film were elaborated through a series of characterizations. Both a low corrosion current density and high charge-transfer impedance are achieved. In addition, a low average corrosion rate was attained in terms of the instantaneous corrosion test together with

immersion evolution tests. It is noted that the pre-made scratches on the surface were effectively self-healed within 24 h of exposure to 0.9 wt % NaCl, which is attributed to the strong chelating tendency of the selected protein molecules to metallic ions. The simple procedure, biocompatibility, and self-healing characteristics render this method applicable to the preparation of anticorrosive or bio-implanted Mg alloys.

Corresponding Author

Qiuming Peng – State Key Laboratory of Metastable Materials Science and Technology, Yanshan University, Qinhuangdao 066004, China; orcid.org/0000-0002-3053-7066;
Email: pengqiuming@ysu.edu.cn

Authors

Jiawen Feng – State Key Laboratory of Metastable Materials Science and Technology, Yanshan University, Qinhuangdao 066004, China; orcid.org/0000-0002-0509-6852

Yukun Pan – State Key Laboratory of Metastable Materials Science and Technology, Yanshan University, Qinhuangdao 066004, China

Meng Yang – State Key Laboratory of Metastable Materials Science and Technology, Yanshan University, Qinhuangdao 066004, China

Carlos Fernandez – School of Pharmacy and Life Sciences, Robert Gordon University, Aberdeen AB107GJ, U.K.

Xiaobo Chen – School of Engineering, RMIT University, Carlton 3053 VIC, Australia; orcid.org/0000-0002-4508-5971

Author Contributions

The manuscript was written through contributions of all authors. All authors have given approval to the final version of the manuscript. These authors contributed equally.

Notes

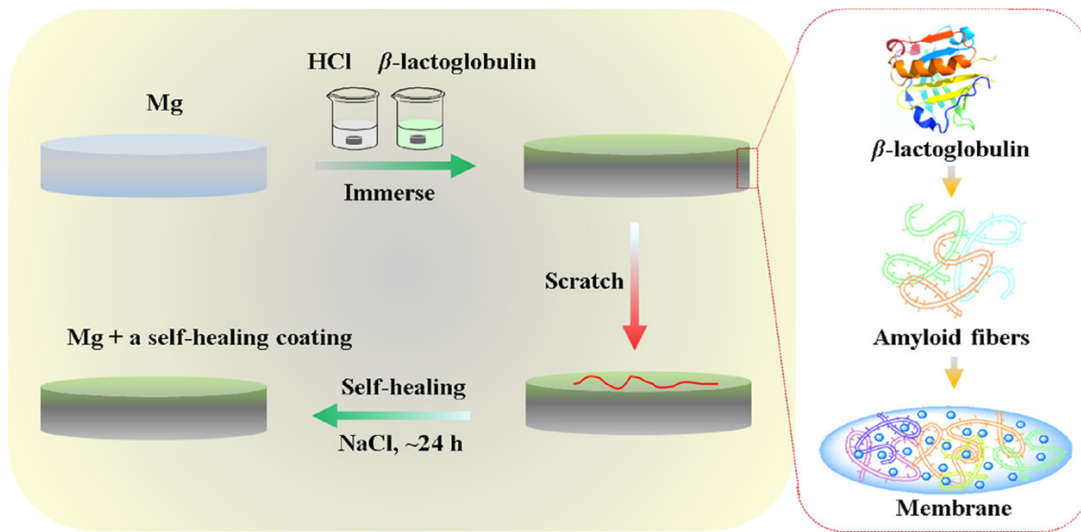
The authors declare no competing financial interest.

The authors greatly acknowledge the financial support from the National Natural Science Foundation-Outstanding Youth Foundation (51771162 and 51971194). We would like to express our gratitude to the Hebei Province Youth Top-notch Talent Program and the Hebei Province Graduate Student Innovation Funding Project Fund (CXZZBS2021122). C.F. would like to express his gratitude to PALS for its support.

REFERENCES

- (1) Cui, X. J.; Lin, X. Z.; Liu, C. H.; Yang, R. S.; Zheng, X. W.; Gong, M. Fabrication and corrosion resistance of a hydrophobic micro-arc oxidation coating on AZ31 Mg alloy. *Corros. Sci.* 2015, 90, 402–412.
- (2) Zhang, F.; Zhang, C. L.; Song, L.; Zeng, R. C.; Li, S. Q.; Cui, H. Z. Fabrication of the Superhydrophobic Surface on Magnesium Alloy and Its Corrosion Resistance. *J. Mater. Sci. Technol.* 2015, 31, 1139–1143.
- (3) Zhao, Y. B.; Shi, L. Q.; Ji, X. J.; Li, J. C.; Han, Z. Z.; Li, S. Q.; Zeng, R. C.; Zhang, F.; Wang, Z. L. Corrosion resistance and antibacterial properties of polysiloxane modified layer-by-layer assembled self-healing coating on magnesium alloy. *J. Colloid Interface Sci.* 2018, 526, 43–50.
- (4) Cao, F. Y.; Shi, Z. M.; Hofstetter, J.; Uggowitzer, P.; Song, G. L.; Liu, M.; Atrens, A. Corrosion of ultra-high-purity Mg in 3.5% NaCl solution saturated with Mg(OH)₂. *Corros. Sci.* 2013, 75, 78–99.
- (5) Ke, C.; Wu, Y. J.; Qiu, Y.; Duan, J. H.; Birbilis, N.; Chen, X. B. Influence of surface chemistry on the formation of crystalline hydroxide coatings on Mg alloys in liquid water and steam systems. *Corros. Sci.* 2016, 113, 145–159.
- (6) Forsyth, M.; Howlett, P.; Tan, S. K.; MacFarlane, D.; Birbilis, N. An Ionic Liquid Surface Treatment for Corrosion Protection of AZ31. *Electrochem. Solid-State Lett.* 2006, 9, No. B52.
- (7) Huo, H. W.; Li, Y.; Wang, F. H. Corrosion of AZ91D magnesium alloy with a chemical conversion coating and electroless nickel layer. *Corros. Sci.* 2004, 46, 1467–1477.

- (8) Zhang, Y. F.; Blawert, C.; Tang, S. W.; Hu, J.; Mohedano, M.; Zheludkevich, M. L.; Kainer, K. U. Influence of surface pre-treatment on the deposition and corrosion properties of hydrophobic coatings on a magnesium alloy. *Corros. Sci.* 2016, 112, 483–494.
- (9) Chong, K. Z.; Shih, T. S. Conversion-coating treatment for magnesium alloys by a permanganate–phosphate solution. *Mater. Chem. Phys.* 2003, 80, 191–200.
- (10) De Witte, A. M. J. C.; De Maeyer, E. A. P.; Verbeeck, R. M. H. Surface roughening of glass ionomer cements by neutral NaF solutions. *Biomaterials* 2003, 24, 1995–2000.
- (11) Mingo, B.; Arrabal, R.; Mohedano, M.; Llamazares, Y.; Matykina, E.; Yerokhin, A.; Pardo, A. Influence of sealing post-treatments on the corrosion resistance of PEO coated AZ91 magnesium alloy. *Appl. Surf. Sci.* 2018, 433, 653–667.
- (12) Pezzato, L.; Brunelli, K.; Napolitani, E.; Magrini, M.; Dabalà, M. Surface properties of AZ91 magnesium alloy after PEO treatment using molybdate salts and low current densities. *Appl. Surf. Sci.* 2015, 357, 1031–1039.
- (13) Chen, F.; Zhou, H.; Yao, B.; Qin, Z.; Zhang, Q. Corrosion resistance property of the ceramic coating obtained through microarc oxidation on the AZ31 magnesium alloy surfaces. *Surf. Coat. Technol.* 2007, 201, 4905–4908.
- (14) Liu, Q.; Chen, D. X.; Kang, Z. X. One-step electrodeposition process to fabricate corrosion-resistant superhydrophobic surface on magnesium alloy. *ACS Appl. Mater. Interfaces* 2015, 7, 1859–1867.
- (15) Pan, Y.; Wu, G.; Huang, Z.; Wu, X.; Liu, Y.; Ye, H. Corrosion behaviour of carbon fibre reinforced polymer-magnesium alloy hybrid laminates. *Corros. Sci.* 2017, 115, 152–158.
- (16) Agarwal, S.; Curtin, J.; Duffy, B.; Jaiswal, S. Biodegradable magnesium alloys for orthopaedic applications: A review on corrosion, biocompatibility and surface modifications. *Mater. Sci. Eng., C* 2016, 68, 948–963.
- (17) Xiong, P.; Yan, J.; Wang, P.; Jia, Z.; Zhou, W.; Yuan, W.; Li, Y.; Liu, Y.; Cheng, Y.; Chen, D.; Zheng, Y. A pH-sensitive self-healing coating for biodegradable magnesium implants. *Acta Biomater.* 2019, 98, 160–173.
- (18) Wang, J. K.; Zhou, Q.; Wang, J. P.; Yang, S.; Li, G. L. Hydrophobic self-healing polymer coatings from carboxylic acid- and fluorine-containing polymer nanocontainers. *Colloids Surf., A* 2019, 569, 52–58.
- (19) Wang, L.; Wang, L.; Zang, L.; Wang, Z.; Elbaz, A.; Zou, Q.; Su, Q.; Zhu, Y.; Che, F. Biocompatibility polyelectrolyte coating with water-enabled self-healing ability. *J. Taiwan Inst. Chem. Eng.* 2018, 91, 130–137.
- (20) Adamcik, J.; Jung, J. M.; Flakowski, J.; De Los Rios, P.; Dietler, G.; Mezzenga, R. Understanding amyloid aggregation by statistical analysis of atomic force microscopy images. *Nat. Nanotechnol.* 2010, 5, 423–428.
- (21) Banfalvi, G. *Cellular Effects of Heavy Metals*; Springer: Dordrecht, 2011.
- (22) Omanovic, S.; Roscoe, S. G. Interfacial Behavior of beta-Lactoglobulin at a Stainless Steel Surface: An Electrochemical Impedance Spectroscopy Study. *J. Colloid Interface Sci.* 2000, 227, 452–460.
- (23) Bryant, C.; McClements, D. Molecular basis of protein functionality with special consideration of cold-set gels derived from heat-denatured whey. *Trends Food Sci. Technol.* 1998, 9, 143–151.
- (24) Tsai, C.; Lin, S.; Wolfson, H.; Nussinov, R. Studies of protein–protein interfaces: A statistical analysis of the hydrophobic effect. *Protein Sci.* 1997, 6, 53–64.
- (25) Jung, J. M.; Savin, G.; Pouzot, M.; Schmitt, C.; Mezzenga, R. Structure of heat-induced beta-lactoglobulin aggregates and their complexes with sodium-dodecyl sulfate. *Biomacromolecules* 2008, 9, 2477–2486.
- (26) Li, C.; Adamcik, J.; Mezzenga, R. Biodegradable nanocomposites of amyloid fibrils and graphene with shape-memory and enzymesensing properties. *Nat. Nanotechnol.* 2012, 7, 421–427.
- (27) Feng, J.; Li, H.; Deng, K.; Fernandez, C.; Zhang, Q.; Peng, Q. Unique corrosion resistance of ultrahigh pressure Mg-25Al binary alloys. *Corros. Sci.* 2018, 143, 229–239.
- (28) Sawaya, M. R.; Sambashivan, S.; Nelson, R.; Ivanova, M. I.; Sievers, S. A.; Apostol, M. I.; Thompson, M. J.; Balbirnie, M.; Wiltzius, J. J.; McFarlane, H. T.; Madsen, A. O.; Riek, C.; Eisenberg, D. Atomic structures of amyloid cross-beta spines reveal varied steric zippers. *Nature* 2007, 447, 453–457.
- (29) Cao, F.; Song, G. L.; Atrous, A. Corrosion and passivation of magnesium alloys. *Corros. Sci.* 2016, 111, 835–845.



Scheme 1 Flow Chart of the Preparation Process of the Lactoglobulin Composite Film

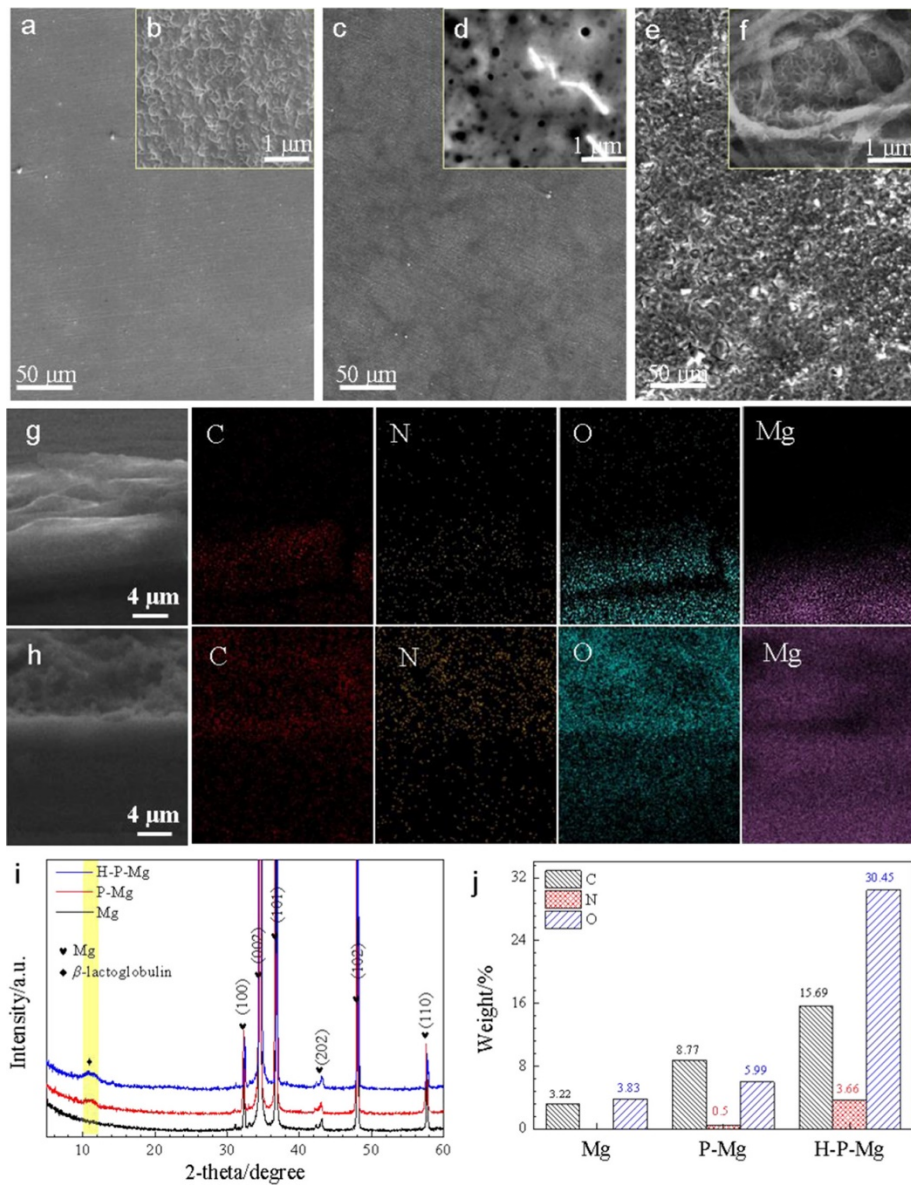


Figure 1. SEM images and phase compositions of different samples. (a, b) Mg; (c, d) P-Mg; and (e, f) H-P-Mg. (g) EDS mapping of the lactoglobulin film for P-Mg and (h) EDS mapping of the lactoglobulin film for H-P-Mg. (i) XRD pattern of three samples. (j) Elemental compositions of three samples.

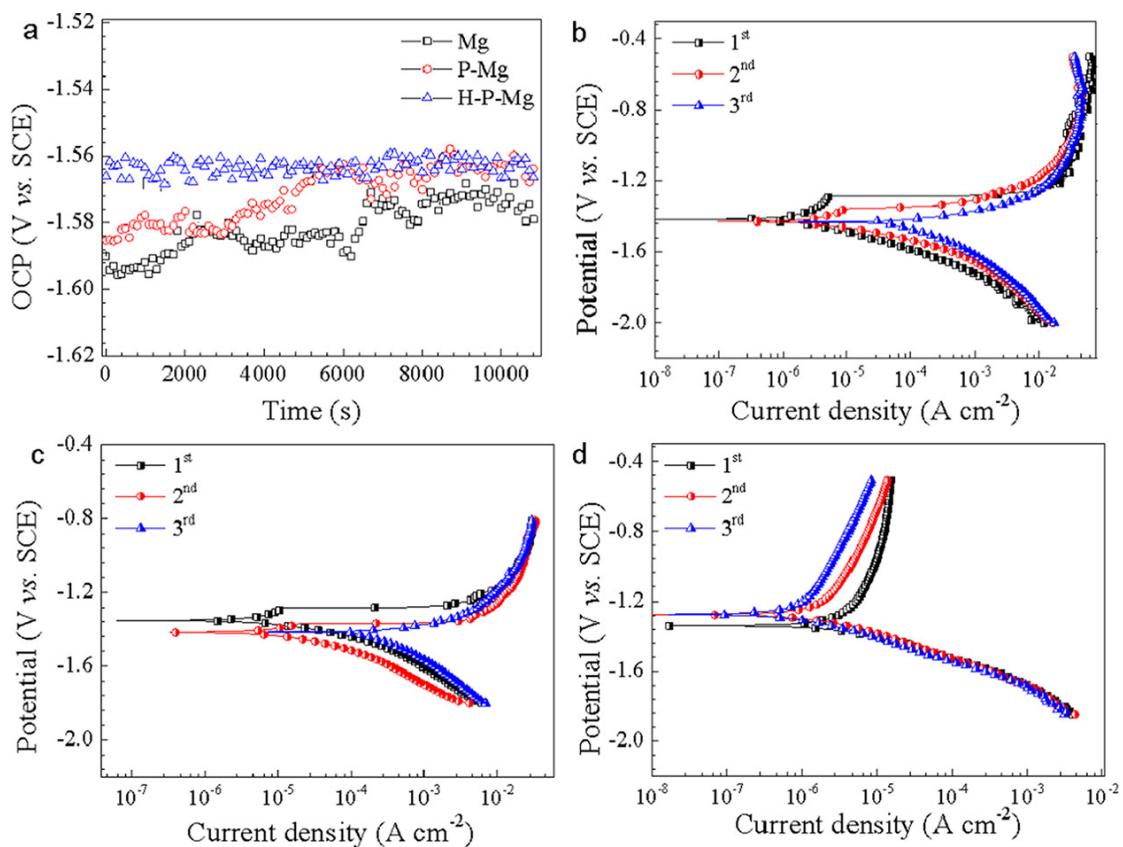


Figure 2. (a) OCP curves of the different samples in a solution of 0.9 wt % NaCl at RT. The three-times polarization curves in a solution of 0.9 wt % NaCl, (b) Mg, (c) P-Mg, and (d) H-P-Mg. The time interval between continuous two tests is 2 h. The scan rate is 0.3 mV/s.

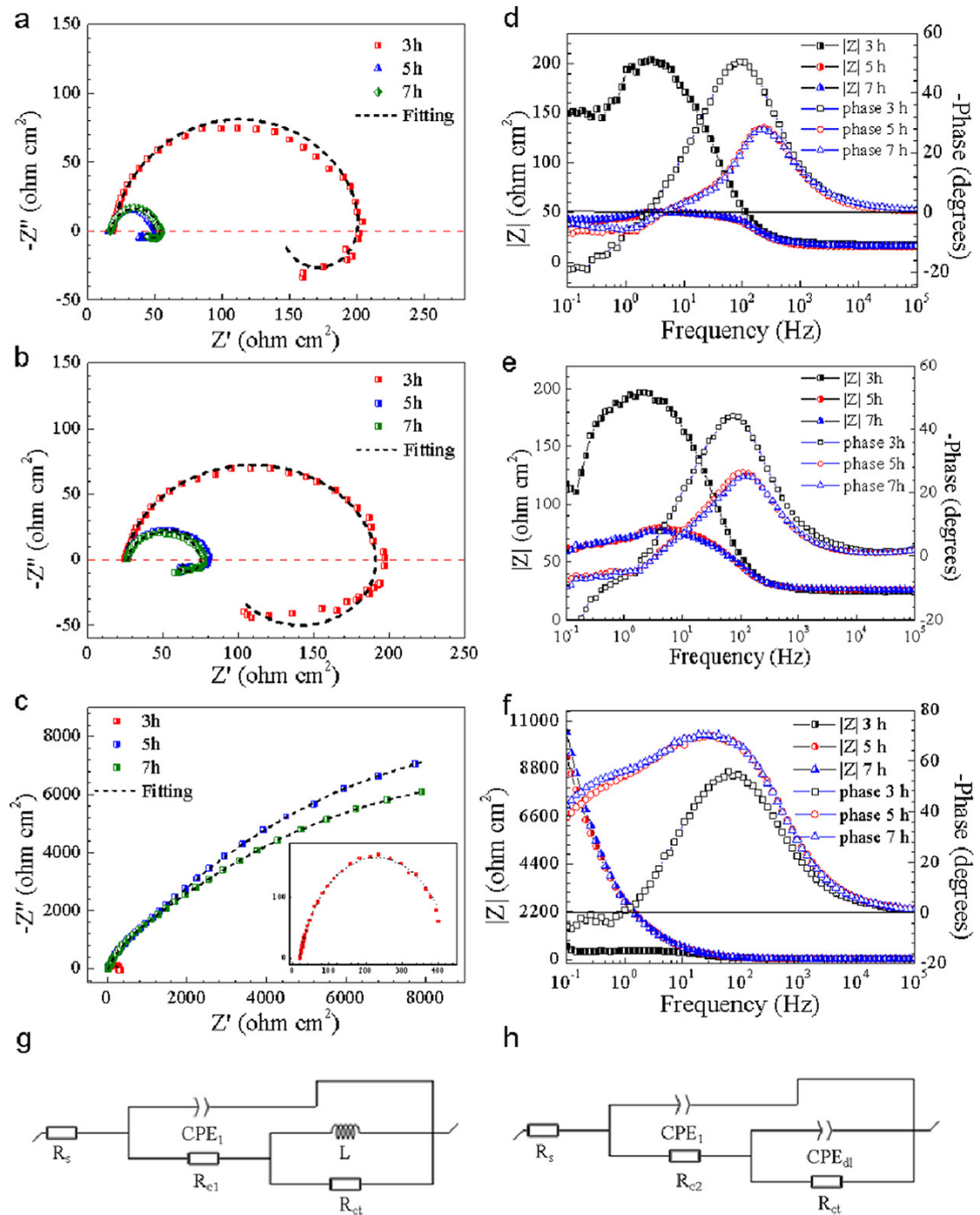


Figure 3. Nyquist curves of the different state samples immersed in a solution of 0.9 wt % NaCl for different immersion times. (a) Mg; (b) P-Mg; and (c) H-P-Mg. Bode spectra corresponding to Nyquist curves: (d) Mg; (e) P-Mg; and (f) H-P-Mg. The equivalent circuit obtained by fitting the Nyquist diagram: (g) Mg and P-Mg; and (h) H-P-Mg.

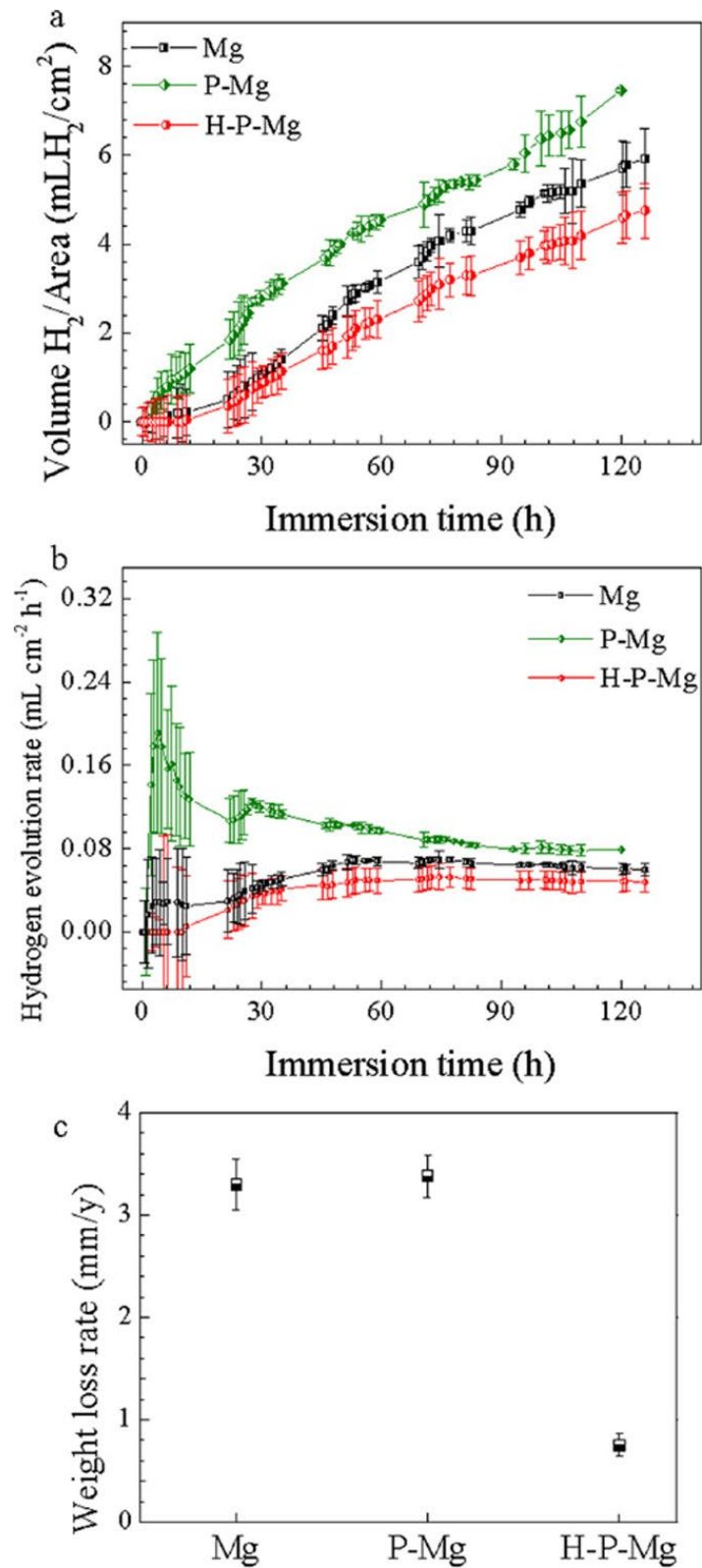


Figure 4. (a) Volume of H₂ dependent on the immersion time. (b) H₂ evolution rate of the different samples. (c) Weight-loss rate of the different samples.

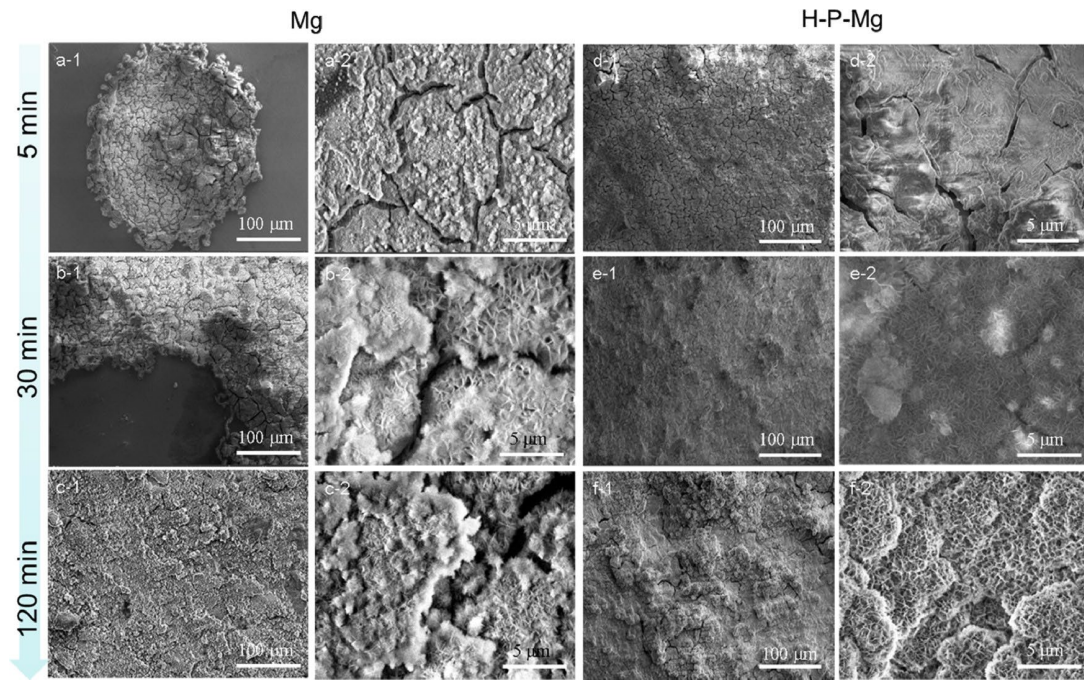


Figure 5. SEM images of the morphology evolution processes of both Mg and H-P-Mg samples during the immersion range of 5-120 min. (a-c) Mg and (d-f) H-P-Mg.

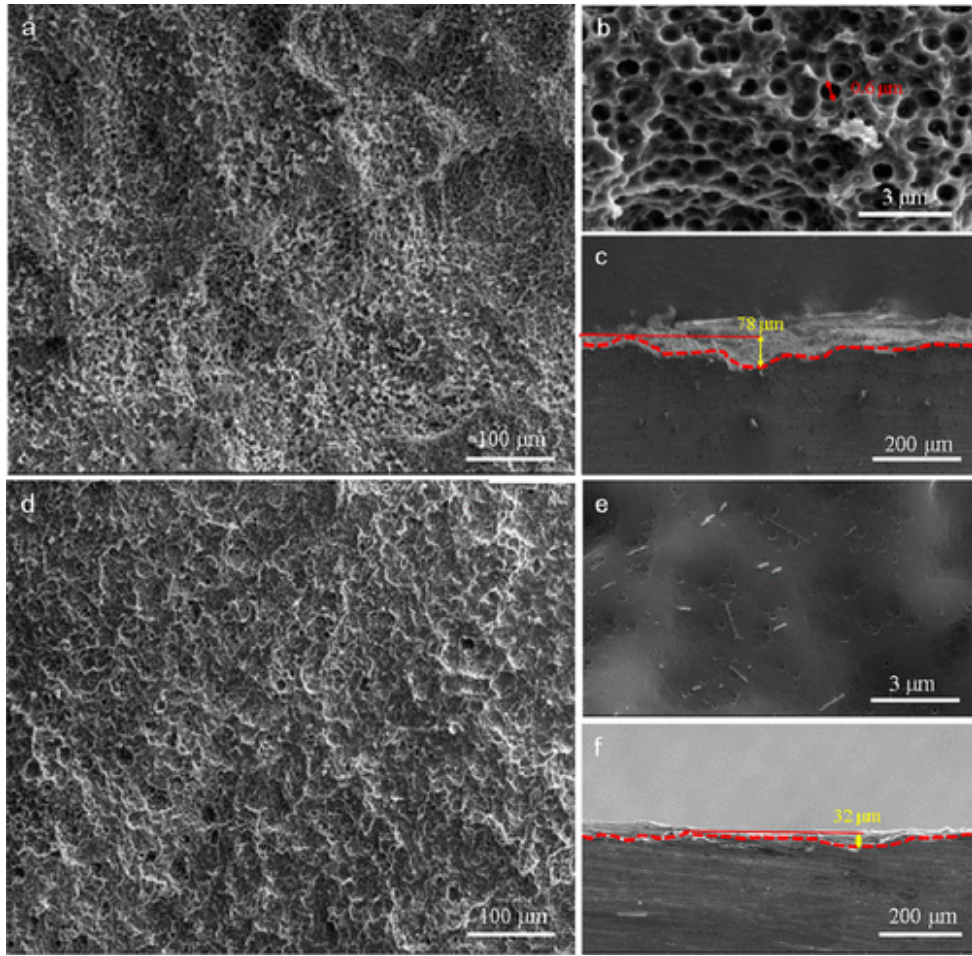


Figure 6. SEM images of the samples after removing corrosion products. (a, b) Surface morphologies of Mg. (c) Sectional view of Mg. (d, e) Surface morphologies of the H-P-Mg. (f) Sectional view of H-P-Mg.

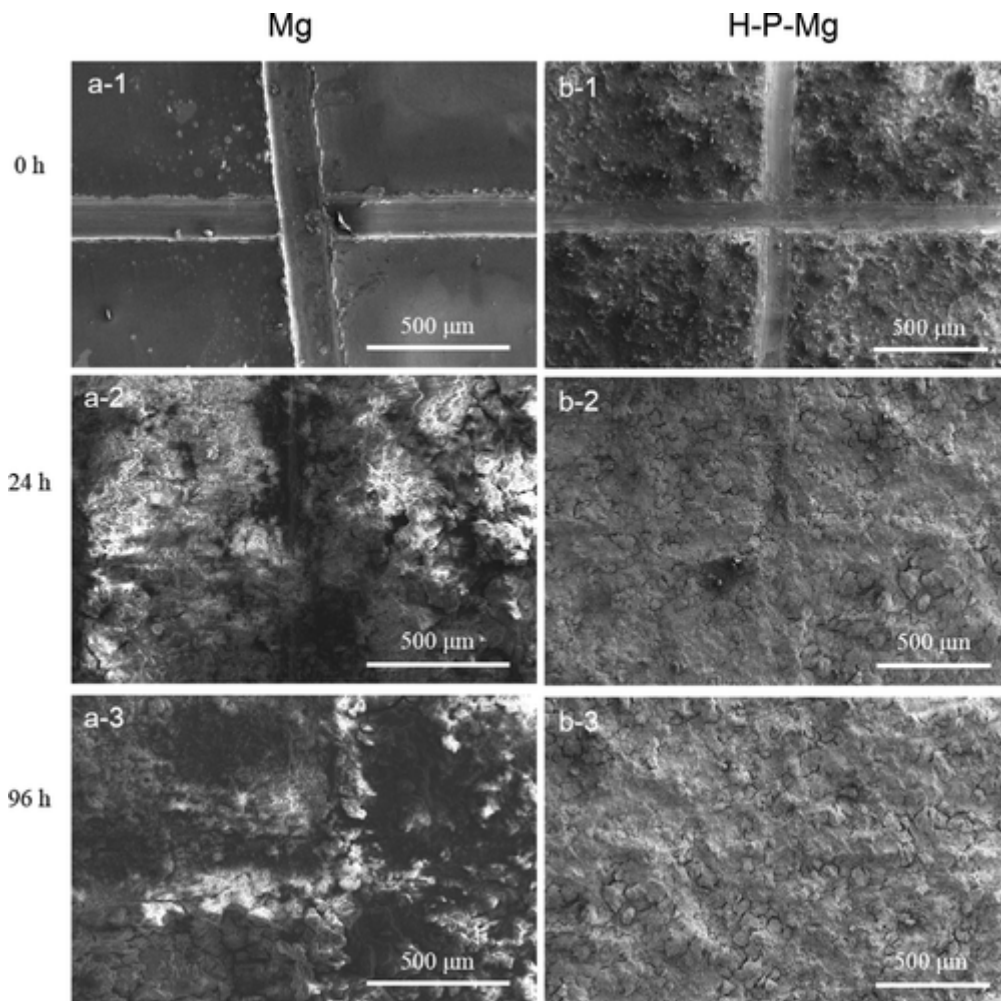


Figure 7. Self-healing observations. ((a-1)–(a-3)) Ex situ SEM images of crack variation on the surface of Mg. ((b-1)–(b-3)) Ex situ SEM images of crack variation on the surface of H-P-Mg.

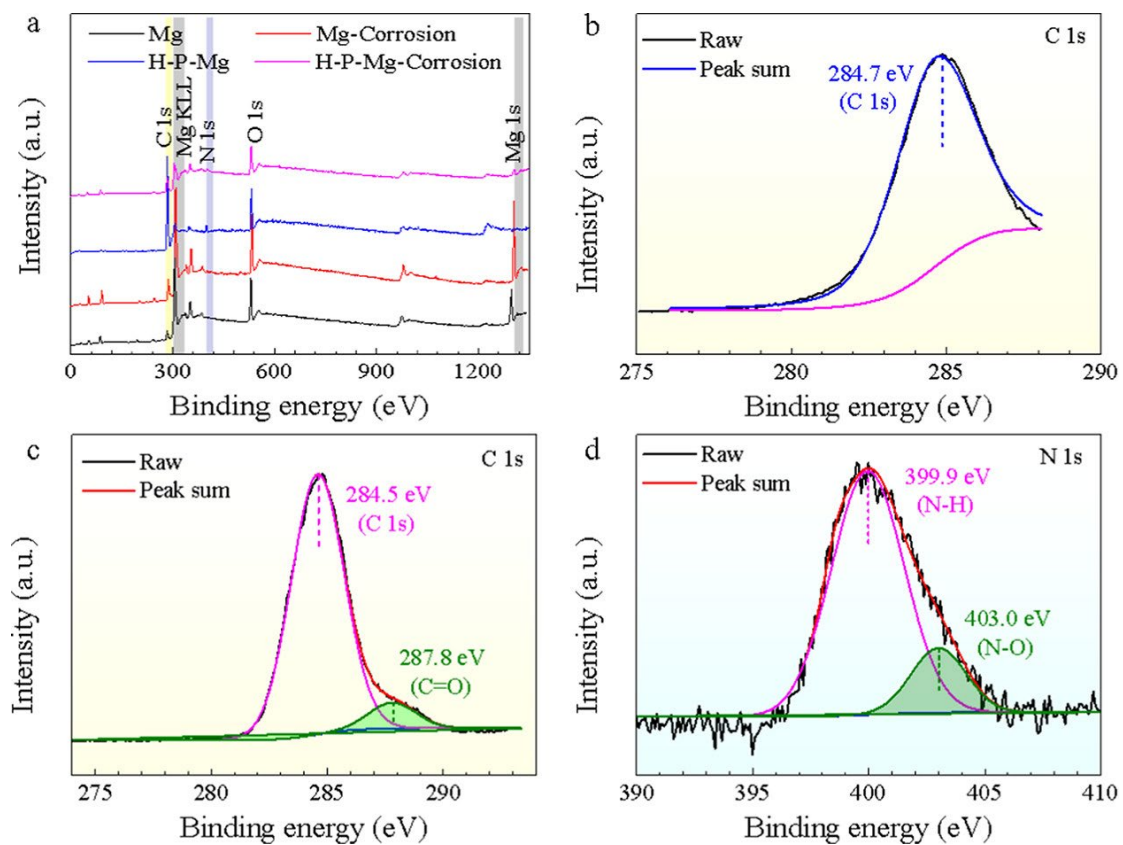


Figure 8. (a) XPS spectra of Mg, H-P-Mg, and their corroded samples immersed in 0.9 wt % NaCl solution. Fitting curves of partial elements: (b) C 1s XPS spectra of Mg and (c) and (d) C 1s and N 1s XPS spectra of H-P-Mg, respectively.

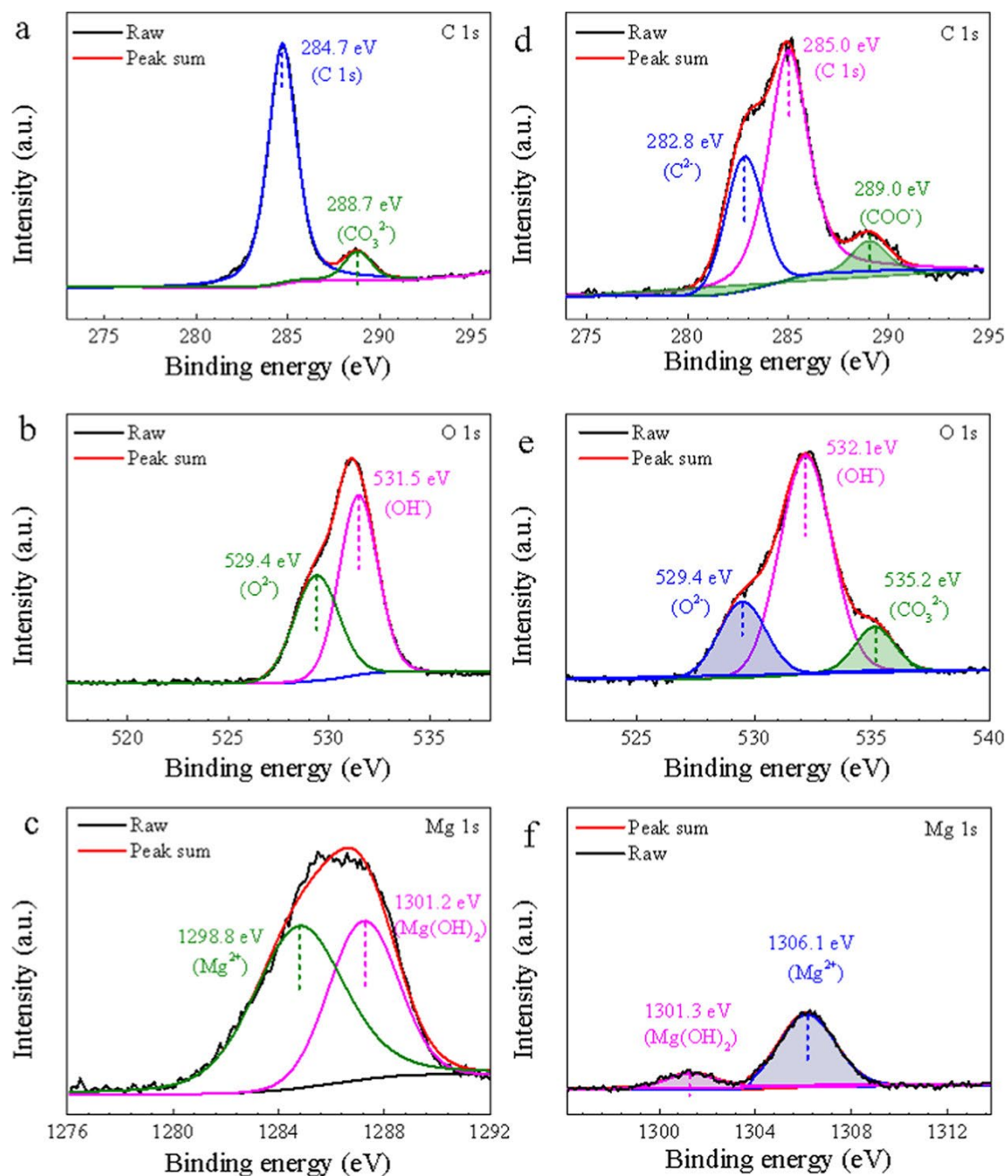


Figure 9. High magnification XPS spectra of (a–c) Mg and (d–f) H-P-Mg immersed in 0.9 wt % NaCl solution.

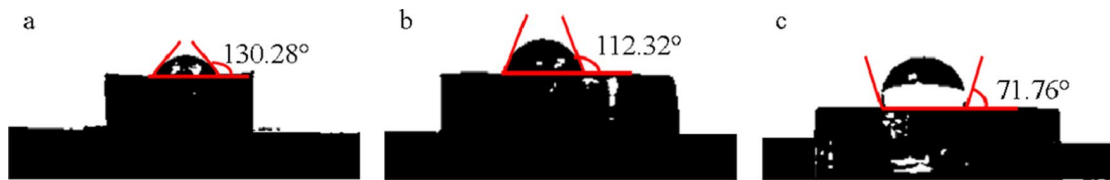


Figure 10. Contact angles of water on the surfaces of alloys. (a) Mg; (b) P-Mg; and (c) H-P-Mg.

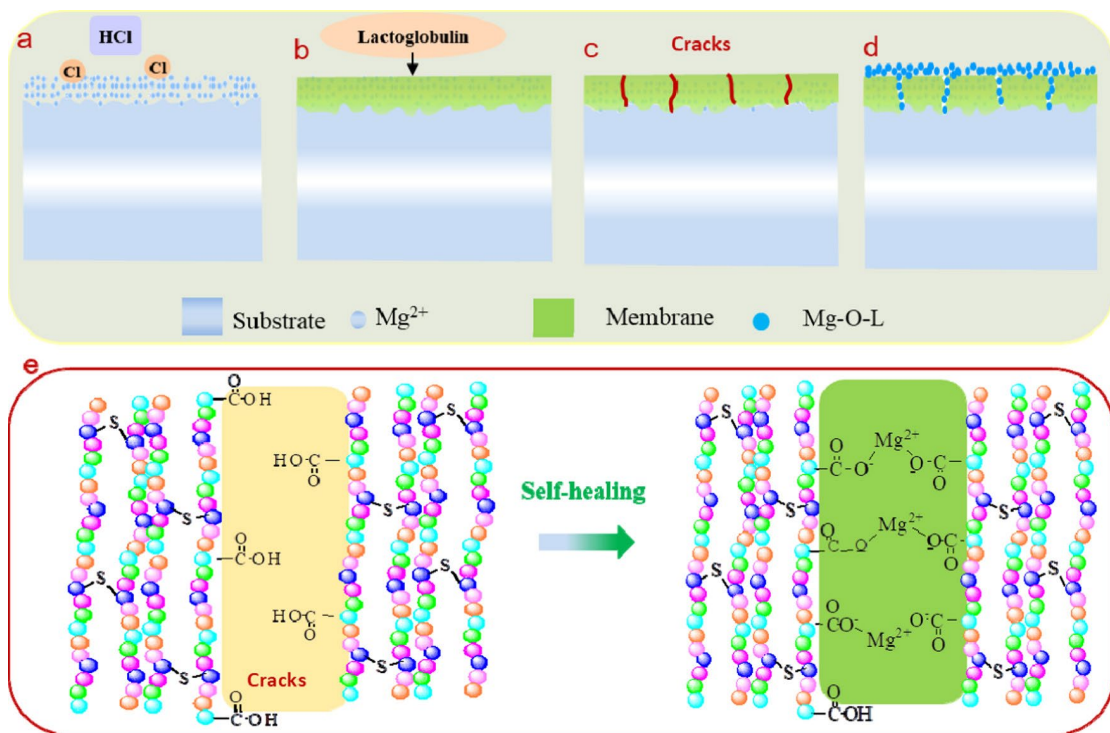


Figure 11. Schematic illustration of the proposed self-healing mechanisms of the lactoglobulin protein-based composite coating. (a-d) Schematic diagram of the macroscopic and (e) Schematic diagram of the microstructure.

Table 1. Parameters Calculated on Tafel Curves

<i>samples</i>	E_{corr} (V_{SCE})	i_{corr} (A/cm^2)	β_a (V)	β_c (V)	P_i (mm/y)
Mg	-1.44 ± 0.16	$2.3 \pm 0.2 \times 10^{-5}$	0.38 ± 0.35	-0.11 ± 0.02	0.52 ± 0.06
P-Mg	-1.39 ± 0.04	$8.3 \pm 0.6 \times 10^{-5}$	0.05 ± 0.02	-0.18 ± 0.04	1.86 ± 0.74
H-P-Mg	-1.28 ± 0.02	$8.4 \pm 0.4 \times 10^{-6}$	0.49 ± 0.03	-0.14 ± 0.01	0.03 ± 0.01

Table 2. Fitting Results of the EIS Curves

<i>samples</i>	time (h)	R_s (ohm cm^2)	CPE_1 ($\mu F cm^{-2}$)	R_c (ohm cm^2)	L (H cm^{-2})	CPE_{dl} ($\mu F cm^{-2}$)	R_{ct} (ohm cm^2)
Mg	3	18.6	56.5	101.9	5179.1		80.9
	5	16.1	52.4	22.6	567.0		11.2
	7	16.8	57.7	24.9	358.7		8.6
P-Mg	3	24.6	67.8	67.0	12878.5		102.5
	5	26.3	94.3	35.6	1229.0		17.3
	7	25.2	90.3	32.4	1288.8		17.0
H-P-Mg	3	19.4	27.8	35.1		20.2	339.9
	5	17.5	47.9	3502.9		92.0	15430.6
	7	18.0	47.7	3781.3		99.2	16633.7